Maximum Wireless Power Transmission Using Real-Time Single Iteration Adaptive Impedance Matching

Fatemeh Nasr Esfahani, *Student Member, IEEE*, Seyed M. Madani, *Senior Member, IEEE*, Mehdi Niroomand, *Member, IEEE*, and Alireza Safaee, *Senior Member, IEEE*

***Abstract*— Wireless power transfer (WPT) systems' efficiency is significantly impacted by non-monotonic variations in the coupling coefficient. For very short distances or strong-coupling cases, the WPT efficiency is minimal at the natural resonant frequency, with two peaks around this frequency, known as the frequency splitting phenomenon. On the other hand, WPT capability decreases for long distances or weak coupling cases. Therefore, adaptive matching is required for WPT systems with varying distances, like wireless charging systems for electric vehicles (EVs). This paper first presents a detailed analysis of the frequency splitting phenomenon by studying the root locations of the WPT system's transfer function. Then, a real-time fixed-frequency adaptive impedance matching (IM) method is proposed, in which the amplitude and phase of the input impedance is estimated using the average active power, the average reactive power, and the amplitude of input voltage. Unlike traditional search-and-find techniques, the proposed method calculates the optimal IM network parameters only in a single iteration, which improves the convergent speed. A scaled-down 20-Watt prototype controlled by the TMSF2812 is fabricated and used to validate the effectiveness of the proposed method over a wide range of coil-to-coil distances.**

***Index Terms*— Wireless power transfer (WPT), inductively-coupled power transfer (IPT), frequency splitting, impedance matching, frequency tracking, electric vehicles (EVs).**

I. Introduction

WIRELESS power transfer (WPT) has attracted a great deal of attention in recent years due to advantages such as convenience, safety, and reliability [1].

WPT has expanded to a wide variety of applications, including medical implants (pacemakers, retinal prosthesis, cochlear implants, etc.) [2], [3], [4], portable consumer electronics (laptops, cell phones, personal digital assistants (PDAs), etc.) [5], and wireless charging of electric vehicles [6], [7], among others.

Manuscript received 7 January 2023; revised 5 May 2023; accepted 26 May 2023. This article was recommended by Associate Editor F. M. Neri. *(Corresponding author: Seyed M. Madani.)*

Fatemeh Nasr Esfahani, Seyed M. Madani, and Mehdi Niroomand are with the Department of Electrical Engineering, University of Isfahan, Isfahan 8174673441, Iran (e-mail: f.nasresfahani@lancaster.ac.uk; madani104@yahoo.com; mehdi_niroomand@eng.ui.ac.ir).

Alireza Safaee was with Bombardier Transportation, Kingston, ON K7K 2H6, Canada. He is now with Osram Sylvania, Wilmington, MA 01887 USA (e-mail: az_safaee@ieee.org).

Color versions of one or more figures in this article are available at https://doi.org/10.1109/TCSI.2023.3284218.

Digital Object Identifier 10.1109/TCSI.2023.3284218

In terms of coil-to-coil distance, At the critical-coupling region [8], the input impedance of the WPT system is almost matched with the impedance of the input power supply [1], [9], [10]. Outside the critical-coupling region, a larger coil-to-coil distance degrades the power delivery due to the lower coupling factor (in the weakly-coupled region) [11]. Also, when the coil-to-coil distance decreases below the critical distance, the coupling factor becomes large and results in an unexpected reduction of the efficiency of power transmitted η_{WPT} due to the frequency splitting phenomenon (in the strongly-coupled region) [8], [12], [13], [14].

To compensate for η_{WPT} reduction, a range-adaptive control technique can be employed, especially for the short coil-to-coil distance cases, where a large impedance mismatch occurs. Two main compensation methods are reported in the literature: (i) frequency tracking approaches in which the input power supply frequency is adjusted adaptively to the coil-to-coil distance [12], [13], [15], [16], [17], [18], [19], and (ii) impedance matching (IM) techniques, such as coupling manipulation [8], [10], [11], lossless IM-networks [1], [2], [9], and IM ability of DC/DC converters [20]. In [15], the reference value for the WPT system input voltage against coupling variations was achieved by tracking split frequencies in the strongly coupled region using a Voltage Controlled Oscillator (VCO). To track the maximum power transmitted point, manual and automatic frequency control of the input power supply were employed in [13] and [19], respectively. Another automated frequency control technique was introduced in [16], which monitored η_{WPT} using out-band wireless communication and adjusted the frequency of the input power supply using a Phase-Locked Loop (PLL) to achieve η_{WPT} goal higher than 70%. In addition, a power-level tracking method adaptive to output power feedback was put forward [21]. It was claimed in [18] that by applying the frequency tracking method, the maximum power could be transmitted just in the strongly coupled region, and beyond this region, there is a drastic decrease of η_{WPT}, so a modified frequency tracking method with a complex load matched was introduced to achieve a stable η_{WPT} beyond this region. To maximize η_{WPT}, an enhanced control algorithm (eCAP) was presented, which tracked the desired operating frequency of the primary power amplifier [17]. However, one drawback of frequency tracking methods can be the considerable reduction of η_{WPT}

outside of the strongly coupled region [18]. They may also call for additional frequency tracking circuits [16], [21], [22]. Impedance matching using coupling manipulation is commonly implemented by adding extra looped coils between coupled coils [10], [23]. Authors in [11] presented an optimally designed antiparallel structure containing forward and reverse coils at the transmitter side for uniform η_{WPT} according to coil-to-coil distance; the problem with coupling manipulation methods is that the input impedance cannot be matched at a wide range of coil-to-coil distances. By analyzing a buck-boost converter in discontinuous conduction mode (DCM), authors in [20] concluded that the input resistance of this converter is independent of the output load and the input voltage of the converter, so a constant η_{WPT} over an extremely wide load range can be achieved. However, they had not verified their method against coupling variations. To maximize η_{WPT} at constant output voltage against coupling and load variations, duty cycles (D) of two DC/DC converters inserted at the transmitter and receiver sides had been adjusted by applying a maximum η_{WPT} point tracking (MEPT) control scheme [22]. However, adding DC/DC converters would increase the losses of the WPT system. In addition, the Zero-Phase-Difference Capacitance Control (ZPDCC) method, targeting a zero phase difference between the input voltage and current signals, has been presented in [24], which uses compensating capacitors as variable capacitors.

In the previously presented impedance matching methods using lossless LC-circuits, the IM networks have been designed for a specific type of input impedance [10]. On the other hand, their optimum IM network parameters had been obtained using time-consuming search-and-find techniques such as Binary Search Algorithm [1] and Genetic Algorithm (GA) [2]. This paper proposes a real-time adaptive impedance matching method in which, firstly, the amplitude and phase of the WPT system's input impedance are obtained using the magnitude of the input voltage of the WPT system and the average valus of active and reactive powers. Then, the value of the IM-network parameters is calculated. This method is applicable to a wide range of coil-to-coil distances (ranging from strongly coupled region to weakly coupled region) and load power factors.

The paper is organized as follows: in section II, the fundamental equations of power transfer for a two-coil WPT system are derived, and the WPT system operation in different coil-to-coil distance ranges is investigated. Moreover, a new analysis of the frequency splitting phenomenon is presented in this section. To extract the values of IM network parameters, section III presents an estimation of the amplitude and phase of the WPT system input impedance. Section IV verifies the proposed method using simulations and experiments. Finally, conclusions are drawn in section VI.

All in all, the main contributions of this manuscript can be divided into two parts:

- In-depth analysis of the frequency splitting phenomenon (an engineering insight into the phenomenon)
- An adaptive IM method (a single-iteration method for maximizing wireless power transfer efficiency at the resonant frequency)

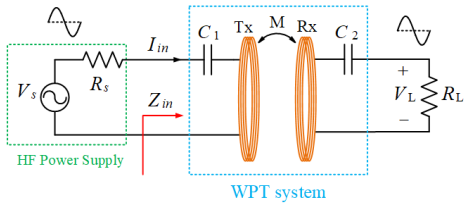

Fig. 1. WPT system equivalent-circuit.

II. WPT System Overview

A. Circuit Modelling

Fig. 1 shows the equivalent circuit of a WPT system with two coils which share a mutual inductance (dependent on the geometry of the coils and the distance between them). The transmitter coil (Tx-coil) is modelled as an inductor L_1 series with its parasitic resistance R_1 being driven by a high frequency (HF) power supply having finite internal resistance R_s. The receiver coil (Rx-coil) is defined similarly, where R_L is the load resistance [25]. It must be mentioned that since the operating frequency has minor variations (less than 1%), it is assumed in this paper that the operating frequency is constant. Therefore, First Harmonic Approximation (FHA) and time-domain analyses yield almost the same result [26].

The governing equations are [8], [10]:

$$\begin{bmatrix} V_s \\ 0 \end{bmatrix} = \begin{bmatrix} Z_1 + R_s & j\omega_s M \\ j\omega_s M & Z_2 + R_L \end{bmatrix} \begin{bmatrix} I_1 \\ I_2 \end{bmatrix} \tag{1}$$

$$\begin{cases} Z_1 = R_1 + j\omega_s L_1 + 1/(j\omega_s C_1) \\ Z_2 = R_2 + j\omega_s L_2 + 1/(j\omega_s C_2) \end{cases} \tag{2}$$

$$\omega_s = 2\pi f_s \tag{3}$$

$$k = M/\sqrt{L_1 L_2}, \quad 0 < k < 1, \tag{4}$$

where ω_s and V_s represent the operating frequency and the root mean square (RMS) of the input voltage, respectively. k represents the coupling coefficient. If the two resonating coils are adjusted at the same frequency, energy can be effectively exchanged with greater efficiency; hence, the resonant series capacitors C_1 and C_2 are chosen to compensate L_1 and L_2 inductances, respectively, at ω_s as follows:

$$C_1 = 1/\omega_s^2 L_1 \ ; \ C_2 = 1/\omega_s^2 L_2 \tag{5}$$

By extracting the currents flowing through the coupled-coils in (6), the voltage gain V_L/V_s is calculated as (7) [27]:

$$\begin{cases} I_1 = \dfrac{(Z_2 + R_L)}{(Z_1 + R_s)(Z_2 + R_L) + (\omega_s M)^2} V_s \\ I_2 = \dfrac{-j\omega_s M}{(Z_1 + R_s)(Z_2 + R_L) + (\omega_s M)^2} V_s \end{cases} \tag{6}$$

$$\left| \frac{V_L}{V_s} \right| = \frac{\omega_s M R_L}{(Z_1 + R_s)(Z_2 + R_L) + (\omega_s M)^2} \tag{7}$$

The wireless power transfer efficiency η_{WPT} is:

$$\eta_{WPT} = \frac{P_{Load}}{P_{in}} = \frac{|V_L|^2/2R_L}{(|V_s - R_s I_1|)^2/2R_{in}}, \tag{8}$$

where R_{in} is the input resistance of the WPT system.

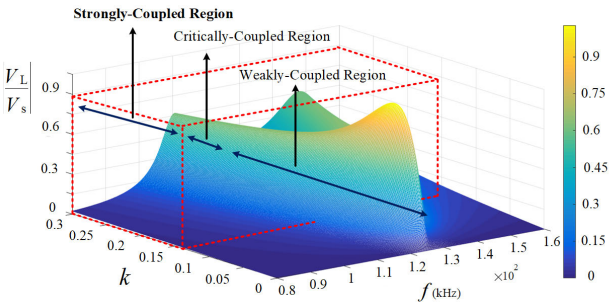

Fig. 2. Simulation results: $|V_L/V_s|$ for different frequencies and coupling coefficients k.

TABLE I
SYSTEM PARAMETERS VALUE

Parameter	Value	Parameter	Value
f_s	125 kHz	C_1	15.83 nF
L_1	101.4 μH	C_2	17.87 nF
L_2	90.7 μH	V_s	14.28V
R_1	0.45 Ω	R_s	1.2 Ω
R_2	0.45 Ω	R_L	10 Ω

B. WPT System Operation in Different Distance Ranges

In WPT systems, the critical-coupling distance between these coils is the longest distance in which the maximum power can be transferred at the natural resonant frequency of the coupled coils [8]. Considering the two-coil WPT system (in Fig. 1) and solving the equation $\partial|V_L/V_s|/\partial k = 0$ at the natural resonant frequency of the coupled-coils f_s, the critical-coupling k_c is [13]:

$$k_c = \frac{1}{2\pi f_s}\sqrt{\frac{R_1(R_2+R_L)}{L_1L_2}} \tag{9}$$

If the coupling-coefficient k deviates from k_c, the efficiency η_{WPT} decreases. In coil-to-coil distances shorter than critical-distance d_c, there are two peaks in the η_{WPT} function occurring in the frequencies different from the coupled coils' natural resonant frequency f_s, due to the frequency splitting phenomenon [8], [12], [13], [15]. Also, at the distances beyond d_c, the coupling-coefficient and thus η_{WPT} decrease. For the system parameter values in Table I, Fig. 2 shows $|V_L/V_s|$ for a range of frequencies and coupling coefficients. This figure clearly shows how the frequency splitting phenomenon happens when coupling-coefficient k is increasing. As k decreases, two splitting frequencies (peaks) approach each other toward the resonant frequency f_s. WPT systems with k larger or smaller than k_c are known as "strongly-coupled"or "weakly-coupled", respectively.

The input impedance of the two-coil WPT system Z_{in} in Fig. 1 is obtained as follows:

$$Z_{in} = Z_1 + \frac{(\omega_s M)^2}{Z_2 + R_L} = R_{in}(\omega_s) + jX_{in}(\omega_s) \tag{10}$$

Based on the maximum power transfer theorem, to reach the maximum wireless transmitted power as (12), the following condition must be held:

$$R_{in}(\omega_s) = R_s \;;\; X_{in}(\omega_s) = 0 \tag{11}$$

$$P_{in(max)} = R_{in}I_{in}^2 = R_{in}\left(\frac{V_s}{R_{in}+R_s}\right)^2 = \frac{V_s^2}{4R_{in}} \tag{12}$$

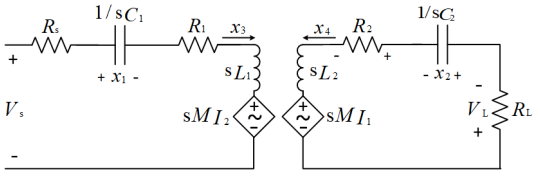

Fig. 3. Equivalent circuit of WPT system for steady-state analysis.

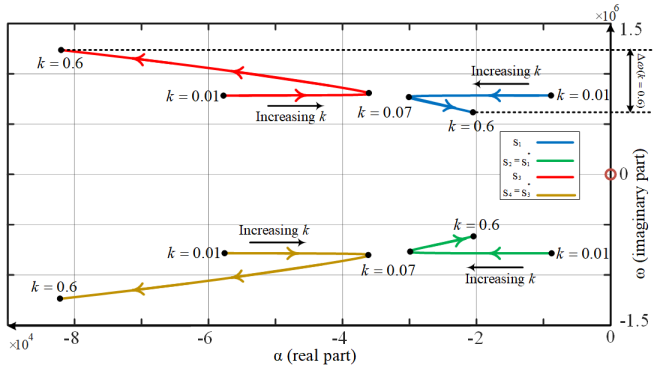

Fig. 4. Root locations versus coupling-coefficient k variation.

C. Detailed Analysis of the Frequency Splitting Phenomenon

General state-space representation is used to extract the transfer function in the two-coil WPT system with the equivalent circuit shown in Fig. 3:

$$\dot{x}(t) = Ax(t) + Bu(t), \tag{13}$$

where $x(t) = [x_1, x_2, x_3, x_4] = [v_{C1}, v_{C2}, i_{L1}, i_{L2}]$ is the space vector, and the input vector $u(t)$ is equal to $v_s(t) = V_s Sin(\omega_s t)$.

The state equations are:

$$\begin{cases} (R_1+R_s)x_3 + x_1 + L_1\dot{x_3} + M\dot{x_4} = u \\ (R_2+R_L)x_4 + x_2 + L_2\dot{x_4} + M\dot{x_3} = 0 \\ x_3 = C_1\dot{x_1} \;;\; x_4 = C_2\dot{x_2} \end{cases} \tag{14}$$

The system transfer function $G(s) = V_L(s)/V_s(s)$ from the input voltage $v_s(t)$ to the output voltage (load voltage) $v_L(t)$ is found as below:

$$G(s) = \frac{MR_Ls^3}{s^4M^2 + (s^2L_1 + sR_1' + 1/C_1)(s^2L_2 + sR_2' + 1/C_2)}, \tag{15}$$

where $s = j\omega$, $R_1' = R_1 + R_s$, and $R_2' = R_2 + R_L$.

At short transfer distance (large M), the denominator has 4 roots as:

$$\begin{cases} s_{1,2} = \alpha_1 \pm j\omega_1 \\ s_{3,4} = \alpha_2 \pm j\omega_2 \end{cases} \tag{16}$$

Fig. 4 shows these roots as functions of the coupling coefficient k. As seen, while increasing k, the imaginary parts of these roots are separating from each other, resulting in the separation of two splitting frequencies, f_{odd} and f_{even}. When k decreases, two splitting frequencies merge to the resonant frequency of the coupled coils f_s.

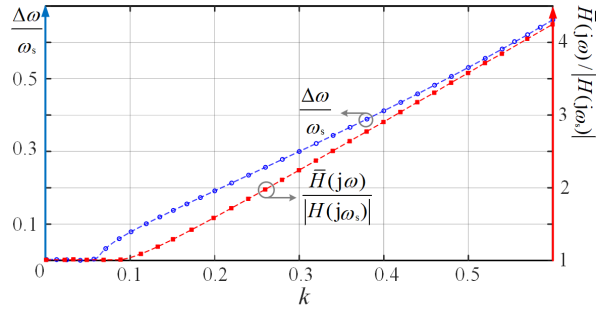

Fig. 5. $\Delta\omega/\omega_s$ and $\bar{H}(j\omega)/|H(j\omega_s)|$ versus coupling-coefficient k variation.

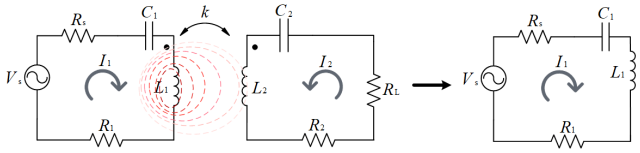

Fig. 6. Two-coil WPT system at weakly-coupled region.

On the other hand, when M is small, the denominator of $G(s)$ in (17) has only two roots, the natural resonant frequency of the coupled coils.

$$G(s) = \frac{M R_L s^3}{(s^2 L_1 + s R_1' + 1/C_1)(s^2 L_2 + s R_2' + 1/C_2)} \tag{17}$$

To clarify more, the peak and frequency separations are plotted as functions of k in Fig. 5, where $\Delta\omega$ and $\bar{H}(j\omega)$ are as follows:

$$\Delta\omega = \omega_{odd} - \omega_{even} \tag{18}$$

$$\bar{H}(j\omega) = (|H(j\omega_{odd})| + |H(j\omega_{even})|)/2 \tag{19}$$

1) More Insight Into the Frequency Splitting Phenomenon: (i) At *Weakley-coupled region* ($k < k_{critical}$), large transfer distances between the coupled coils, or small k, as seen in Fig. 6, only a small part of the alternating magnetic flux $\phi(t)$ generated by the current at the transmitter coil $i_1(t)$ interlinks the receiver coil. The voltage induced on the receiver side is proportional to $i_1(t)$ and has the same frequency as the transmitter side. However, since the interlink between the receiver and transmitter coils is weak, the receiver current does not induce a significant voltage in the transmitter coil. Therefore, the transmitter current is not affected, and the transmitter side can be modelled regardless of the receiver side. Thus, the load power P_L has no effect on the impedance seen from the input source Z_{in} and the transmitter stays at resonant condition in $\omega_s = 1/\sqrt{L_1 C_1} = 1/\sqrt{L_2 C_2}$. Therefore, in this case, both transmitter and receiver operate at the resonant condition at ω_s, and there is little impedance mismatching at the transmitter and receiver sides.

(ii) At *Strongly-coupled region* ($k > k_{critical}$) or short transfer distances between the coupled coils, $i_1(t)$ generates an alternating magnetic flux $\phi(t)$, and a significant part of this flux interlinks the receiver coil (see Fig. 7), which induces a voltage across the receiving coil, leading to a current $i_2(t)$ in the receiver coil. In this case, the receiver current produces a significantly induced voltage at the transmitter coil, affecting the resonant frequency of the transmitter and receiver coils.

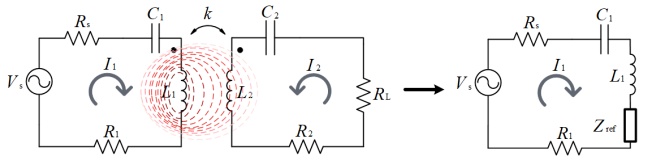

Fig. 7. Two-coil WPT system at strongly-coupled region.

In this case, the reflected impedance from the receiver side Z_{ref} to the transmitter side is significant, which shifts the resonant frequencies at both sides from ω_s. Therefore, there is an impedance mismatch at the input (or the output) of the WPT system, and a local minimum has been observed in power transmission characteristics at the resonant frequency ω_s.

III. The Proposed IM Method

As discussed before, decreasing the coil-to-coil distance increases coupling-coefficient k and impedance mismatch. This paper proposes a method that matches the input impedance of the WPT system Z_{in} with the internal resistance of the HF power supply R_s for wide ranges of distances and all types of load power factors. To determine optimal IM network parameters (L_s, C_p), the input impedance Z_{in} should be estimated in each time instance. This impedance is a function of mutual inductance between the coupled coils M, load impedance R_L, and the HF power supply frequency f_s. The estimation of the input impedance Z_{in} needs voltage and current phasors at the WPT system's input. However, since WPT systems' operating frequencies range from hundreds of kHz up to several MHz, the phasor estimation of voltage and current needs very high sampling rates, which is practically difficult. This paper estimates Z_{in} based on processing analog signals of active power P_{in}, reactive power Q_{in}, and the amplitude of WPT system input voltage $|V_{in}|$.

A. Real-Time Calculation of The WPT System Input Impedance Based on Active and Reactive Power

As mentioned in Section II, it is assumed that voltage and current signals are sinusoidal. As shown in Fig. 8, the instantaneous active power can be calculated as:

$$p_{in}(t) = v_{in}(t) * i_{in}(t) \tag{20}$$

The instantaneous power $p_{in}(t)$ has an average (dc) component $P_{in}(t)$ and an ac component with frequency of $2f$. The average power $P_{in}(t)$ is extracted using a low-pass filter (LPF):

$$P_{in}(t) \triangleq \frac{1}{T}\int_{t-T}^{t} p_{in}(t)\, d(t) \cong LPF\{p_{in}(t)\} \tag{21}$$

An analogue multiplier and LPF with a cut of frequency of $2f/10$ are used in practice. The instantaneous reactive power $q_{in}(t)$ can be expressed as:

$$q_{in}(t) = v_{in}(t - T/4) * i_{in}(t), \tag{22}$$

which needs a phase shifter. Therefore, $Q_{in}(t)$ can be calculated as:

$$Q_{in}(t) \triangleq \frac{1}{T}\int_{t-T}^{t} q_{in}(t)\, d(t) \cong LPF\{q_{in}(t)\} \tag{23}$$

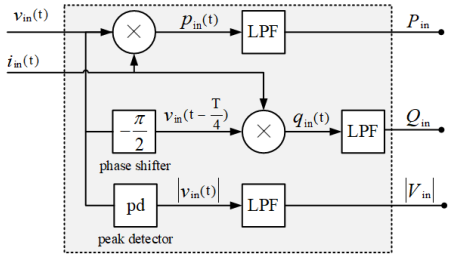

Fig. 8. Extracting diagram for: P_{in}, Q_{in}, and $|V_{in}|$.

Finally, magnitude of the input voltage of the WPT system can be obtained as:

$$|V_{in}| = max\{v_{in}(t')\}, \quad t - T \le t' \le t, \tag{24}$$

this voltage magnitude can be obtained using a peak detector, which contains a diode, smoothing RC and an LPF. Now, to calculate Z_{in}, the following equations are used:

$$S_{in} = V_{in} I_{in}^* = V_{in} \left(\frac{V_{in}}{Z_{in}}\right)^* = \frac{|V_{in}|^2}{Z_{in}^*} \tag{25}$$

$$Z_{in} = \frac{|V_{in}|^2}{S_{in}^*} = \frac{|V_{in}|^2}{P_{in} - jQ_{in}} \tag{26}$$

The amplitude and phase of the WPT system input impedance Z_{in} are as (27) and (28), respectively. As seen, this impedance can be calculated using only the average value of active power P_{in}, reactive power Q_{in}, and magnitude of the input voltage of the WPT system $|V_{in}|$.

$$|Z_{in}| = \frac{|V_{in}|^2}{\sqrt{P_{in}^2 + Q_{in}^2}} \tag{27}$$

$$\angle Z_{in} = \arctan\left(\frac{Q_{in}}{P_{in}}\right) \tag{28}$$

B. Impedance Matching Network Design

Fig. 9 illustrates that the resistive impedance of R_{in} can be conveniently matched to the resistive impedance R_s by adding a shunt capacitor C_p and a series inductance L_s, resulting in motion along with constant-conductance and constant-resistance circles, respectively, both in a clockwise direction. However, when dealing with the practical design and implementation of an IM network for IPT systems, there are some issues to consider; the input impedance of IPT system Z_{in} can be from different types of impedance (resistive R_{in}, resistive-inductive $R_{in} + jXin$, and resistive-capacitive $R_{in} - jXin$), and the designed IM network should be capable of matching all these types of impedance with the impedance of power supply. As can be seen, resistive-inductive and resistive-capacitive impedances can be matched with R_s using the same IM network, with different C_p and L_s values; therefore, the designed IM network can be used for any input impedance.

C. Calculating IM Network Parameters

Fig. 10 shows the equivalent circuit of the two-coil WPT system together with the designed L-matching network,

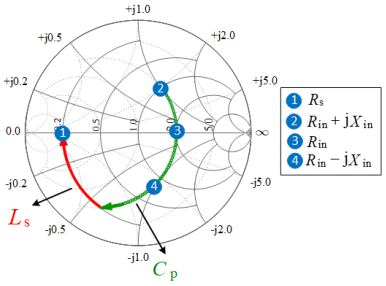

Fig. 9. IM network designed for: (2) resistive-inductive, (3) resistive, and (4) resistive-capacitive input impedance.

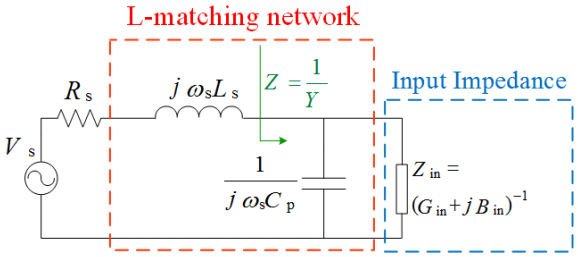

Fig. 10. Equivalent circuit of WPT system with the designed L-matching network.

located between the Tx-coil and HF power supply. This network is used to match the input impedance $Z_{in} = (G_{in} + jB_{in})^{-1}$ with the internal resistance of HF power supply R_s. The impedance Z in Fig. 10 can be calculated as:

$$Z = \frac{1}{Y} = \frac{G_{in}}{G_{in}^2 + (B_{in} + \omega_s C_p)^2} - j\frac{B_{in} + \omega_s C_p}{G_{in}^2 + (B_{in} + \omega_s C_p)^2} \tag{29}$$

To match the impedance Z with $R_s + j\omega_s L_s$, the following condition must be held:

$$Z = (R_s + j\omega_s L_s)^*, \tag{30}$$

which results in:

$$\begin{cases} C_p = \dfrac{1}{\omega_s}\left(\sqrt{\dfrac{G_{in} - R_s G_{in}^2}{R_s}} - B_{in}\right) \\ L_s = \dfrac{1}{\omega_s}\left(\dfrac{B_{in} + \omega_s C_p}{G_{in}^2 + (B_{in} + \omega_s C_p)^2}\right) \end{cases} \tag{31}$$

In this paper, it is assumed that effective series resistances (ESRs) of L_s and C_P are negligible. Otherwise, their impact must be considered in modifying R_s and Z_{in}.

IV. Verification

A. Simulation Study

Simulation results in Fig. 11 illustrate that the proposed IM network increases η_{WPT} (in (8)), especially in the strongly-coupled region with $k = 0.3$, it is improved from less than 60% to about 97% at the natural resonant frequency f_s. In addition, after applying the proposed IM method, η_{WPT} is higher than that of odd or even splitting frequencies.

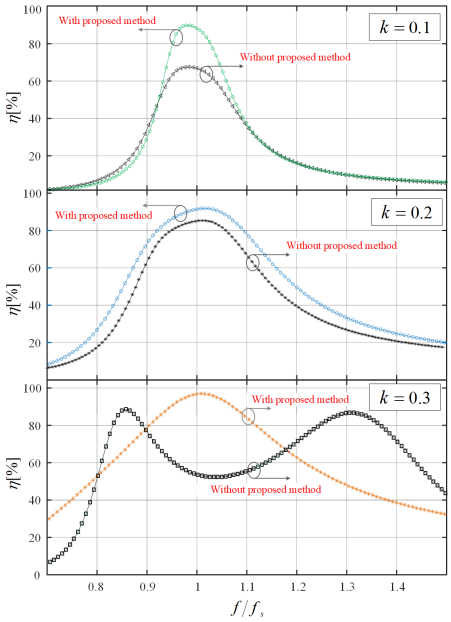

Fig. 11. Efficiency η_{WPT} with and without using the proposed IM method for different coupling coefficients k.

B. Experimental Study

Fig. 12 shows the experimental setup of the implemented WPT system consisting of: an HF power supply, IM network, control circuit, two planar spiral coils, compensating capacitors, and a 10Ω resistance load. The HF power supply is implemented on a PCB using a signal generator (GW INSTEK: GFG-8020H) and a 20Watt linear push-pull power amplifier (using NPN and PNP transistors of TIP35C and TIP36C, respectively), with the output resistance of 1.2Ω. The variable IM network is realized on a PCB using an 8-bit binary capacitor and inductor banks. Both banks are controlled through relay switches (HJR-78F) [1]. The capacitors and the inductors range from 10-1280 nF and 0.1-12.8 μH, respectively. The required L_s and C_p are can be made as follows:

$$\begin{cases} C_P = C_0 \left\{ a_0 2^0 + a_1 2^1 + a_2 2^2 + \ldots + a_7 2^7 \right\} \\ a_0, a_1, a_2, \ldots, a_7 : 0, 1 \\ L_s = L_0 \left\{ b_0 2^0 + b_1 2^1 + b_2 2^2 + \ldots + b_7 2^7 \right\} \\ b_0, b_1, b_2, \ldots, b_7 : 0, 1 \end{cases} \quad (32)$$

Using the above 8-bit capacitor-switches a_i and inductor-switches b_i arrays is common for creating IM network parameters [28]. By choosing the binary values of "0" or "1" for these switches, a capacitor within $10nF$ to $2550nF$ and an inductor within 0.1μH to 25.5μH is available (256 different values for each one), which can be used for various distances/loads. It must be mentioned that the relay-switches are affected by large switching times, and it is suggested to use power MOSFETS. However, the relays have been used in this work as the easiest way to implement and test the proposed IM method.

The IM network is only at the transmitter side between the HF power supply and the Tx-coil, which, as an advantage, avoids wireless communications between transmitter and receiver sides [22].

TABLE II
DETAILED PHYSICAL DIMENSIONS OF THE TWO LITZ-WIRING COILS

Parameter	Value
Inner diameter	8cm
Outer diameter	Tx:19cm and Rx:17cm
Diameter of each wire[a]	$d_2 = 1$mm
Diameter of each wire strand	$d_1 = 0.2$mm
Number of strands n	$n = (d_2/d_1)^2 \cong 24 = 2 \times 12$
Gap between turns	0.5mm
Number of turns	$N_{Tx} = 20$ and $N_{Rx} = 18$

[a]For maximum current of $6A$

To reduce losses associated with the skin and proximity effects at high frequencies, the coils are made by Litz wiring, and their detailed physical dimensions are presented in Table II.

Also, two ceramic capacitors, serving as compensating capacitors, are connected in series with the coupled coils to make them resonate at the frequency of interest f_s. The schematic diagram of the experimental WPT system is depicted in Fig. 13. To obtain the peak (maximum) of input voltage value $|V_{in}|$, first, after measuring the instantaneous value $v_{in}(t)$ via a resistive divider, the peak value of this signal is measured using an analogue peak detector (pd), consisting of a fast-recovery diode (1N5819) and a capacitor. Then, an analogue low pass filter (LPF) is employed to remove its ripples. The current at the input of the Tx-coil $i_{in}(t)$ is measured by using a current transducer (LA 55-P). To calculate $p_{in}(t)$, first, $v_{in}(t)$ and $i_{in}(t)$ are multiplied to each other using an analog multiplier (AD633JN). Then, the average value of active power P_{in} is extracted using an analogue low-pass filter (LPF). Then, the same procedure as that used for extracting P_{in} is employed to extract the average value of reactive power Q_{in}, with the only difference that the inputs of the analogue multiplier are $i_{in}(t)$ and $v_{in}(t - T/4)$. To produce a $(-\pi/2)$ phase shift in $v_{in}(t)$ as $v_{in}(t - T/4)$, an analog circuit containing op-amps (LF353N) and RC filters is employed. Finally, the analog signals P_{in}, Q_{in}, and $|V_{in}|$ are given to the ADC of the DSP (TMS320F2812).

Table III shows the procedure of obtaining optimal IM network parameters C_p and L_s using a DSP; the DSP first calculates the input impedance Z_{in} (using (27) and (28)), then, depending on the load type, obtains IM network parameters (using (31)). Then, appropriate ON/OFF commands are sent to the relay switches. Finally, it is checked whether Z_{in} approaches R_s or not (i.e., $|Z_{in} - R_s| < \varepsilon$). So, this algorithm can be repeated to adapt to new load and distance conditions. In other words, if the coil-to-coil distance d or the output load R_L are changed, (and so $|Z_{in}|$ is changed), the IM network will be provided with new $C_{POptimal}$ and $L_{sOptimal}$.

Using the proposed method, some calculations like peak detecting, multiplying, filtering, and so on are performed in analogue, so the processor with a lower sample rate like AVR can also be used.

By experiments, the coil-to-coil distance $d = 4$cm is found as the critical-distance d_c, for $f_s = 125$kHz. To evaluate the

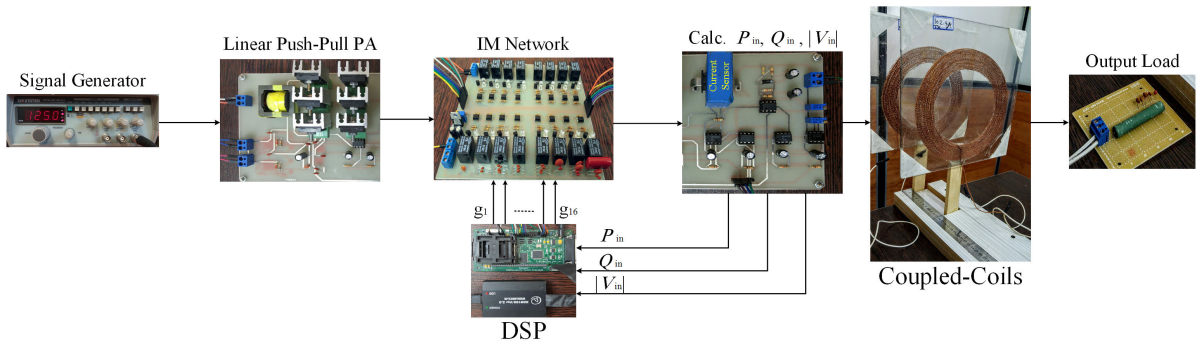

Fig. 12. Experimental setup of the proposed IM method.

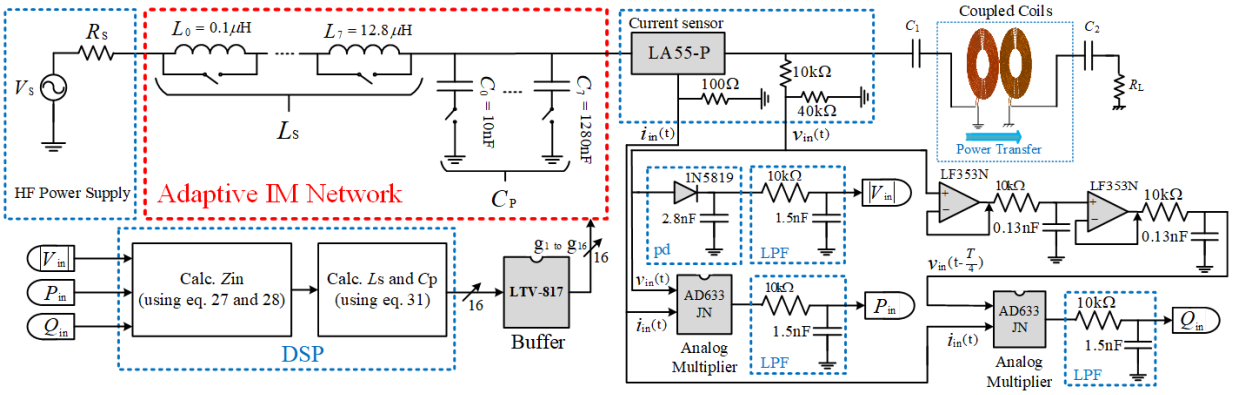

Fig. 13. Schematic diagram of the proposed method.

TABLE III
OBTAINING IM NETWORK PARAMETERS USING DSP

Inputs: R_s , ε
Monitor: P_{in}, Q_{in}, and $|V_{in}|$
Calculate: Z_{in} Using (27) and (28)
Obtain IM network parameters C_P **and** L_s**:**
if $Q_{in} > 0$ (*Resistive-inductive*)
Calculate: C_p and L_s using (31) with $B_{in} < 0$
else if $Q_{in} < 0$ (*Resistive-capacitive*)
Calculate: C_p and L_s using (31) with $B_{in} > 0$
else if $Q_{in} == 0$ (*Resistive*)
Calculate: C_p and L_s using (31) with $B_{in} = 0$
end if
Set: C_P and L_s
Calculate: Z_{in} Using (27) and (28)
if $||Z_{in}| - R_s| < \varepsilon$
$C_{POptimal} = C_P$
$L_{sOptimal} = L_s$
else if $||Z_{in}| - R_s| > \varepsilon$
Return to **Monitor:** P_{in}, Q_{in}, and $|V_{in}|$
end if

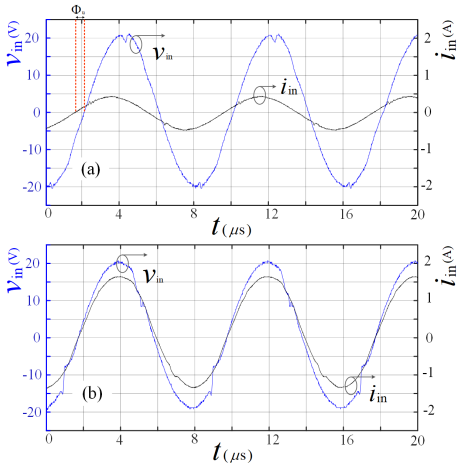

Fig. 14. Experimental results for power factor correction at $d = 2$cm. (a) without impedance matching. (b) with impedance matching.

effectiveness of the proposed method, the current and voltage signals are measured in the strongly coupled region with a coil-to-coil distance of $d = 2$cm.

Fig. 14 illustrates that the adaptive IM method increases the current amplitude and decreases the current-voltage displacement angle ϕ_u to near zero.

Fig. 15 shows the experimental results for the efficiency η_{WPT} when the frequency is swept from 100kHz to 150kHs at coil-coil distances from 1cm to 6cm. This figure shows how the proposed IM method can increase the efficiency η_{WPT}, especially at the natural resonant frequency of the coupled coils.

As mentioned before, the available L_s and C_P from the IM network range from 0.1μH to 25.5 μH and $10n$F to $2550n$F, respectively. Fig. 16 illustrates simulation results for required L_s and C_P when R_L is swept from 0.001Ω to 10kΩ,

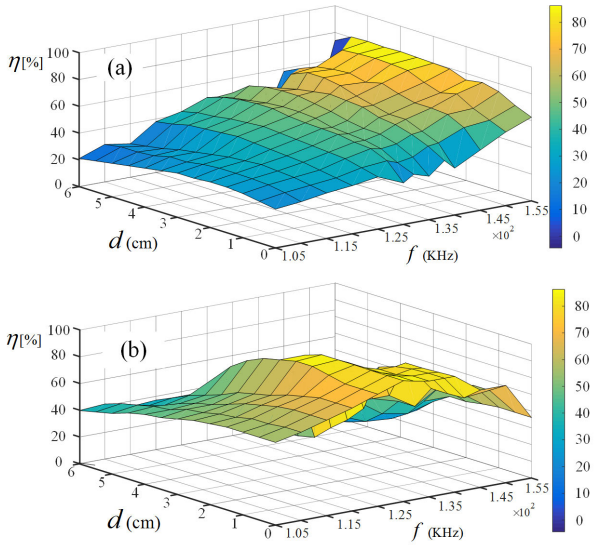

Fig. 15. Experimental results of η_{WPT} for different frequencies and coil-coil distances: (a) before applying the proposed IM method (b) after applying the proposed IM method.

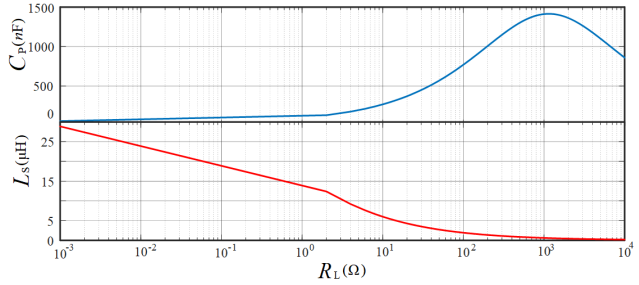

Fig. 16. C_P and L_s pairs corresponding to R_L ranging from 0.001Ω to 10kΩ at $k = 0.3$ ($d \cong 2cm$).

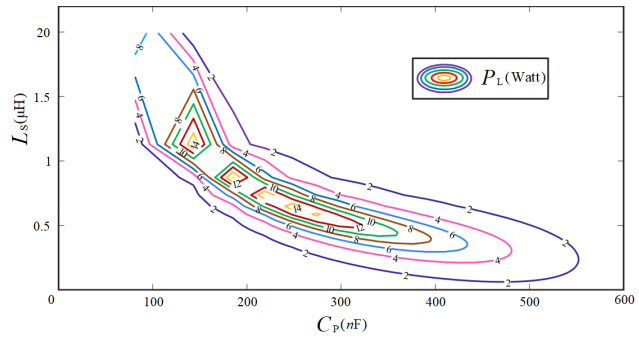

Fig. 17. Output power P_L for C_P and L_s pairs (corresponding to R_L ranging from 0.001Ω to 10kΩ at $k = 0.3$ ($d \cong 2cm$)).

at $d \cong 2cm$ (using eq. (31)). Fig. 17 also shows corresponding variations in P_L. As seen, using the current IM network parameters, it is possible to match the input impedances for R_L more than 0.1 (or the output power P_L less than around 15Watt). In other words, the available L_s causes limitation in the output power, whereas the available C_P does not cause any limitation.

C. Square-Wave Excitation

The source voltage $v_s(t)$ for a square-wave excitation and the input current $i_{in}(t)$ are shown in Fig. 18. As seen, although $v_s(t)$ is a square-wave signal having odd harmonics, $i_{in}(t)$ is almost sinusoidal as a result of capacitors and inductors

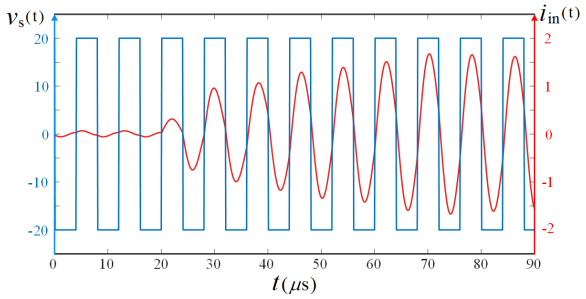

Fig. 18. Simulation results for input source voltage $v_s(t)$ and $i_{in}(t)$ at $k = 0.3$ (The adaptive IM circuit is switched-on from t=20μs).

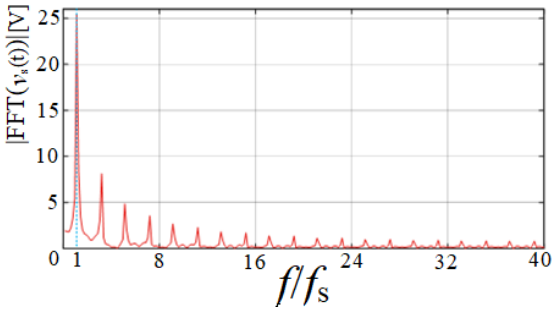

Fig. 19. Fast fourier transformation (FFT) of the source voltage $v_s(t)$ at $k = 0.3$.

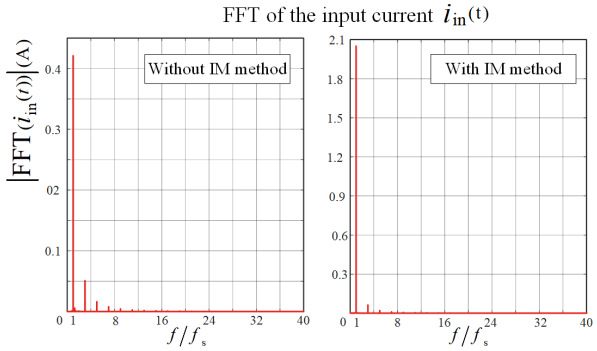

Fig. 20. Fast fourier transformation (FFT) of the input current $i_{in}(t)$, with and without applying the proposed IM method at $k = 0.3$.

employed in the WPT system and IM network. Also, after applying the impedance matching (IM) method, the input current $i_{in}(t)$ amplitude is increased.

The Fast Fourier Transformation (FFT) for the source voltage $v_s(t)$ and the input current $i_{in}(t)$ (with and without applying the IM method) are shown in Fig. 19 and 20, respectively. As can be seen, compared to voltage harmonics, current harmonics are very negligible. Indeed, harmonics of the square-wave voltage decreases by order of harmonics $1/h$. Current harmonics are also decreasing in the same way or even faster. Therefore, the transferred power (which is a multiplication of voltage and current) of each harmonic h, decreases by $1/h^2$ or even faster. Thus, almost all the power is transferred in fundamental harmonic (here is 125kHz). Therefore, almost all the power is transferred via the fundamental harmonic, for both operating states of with and without applying the IM method.

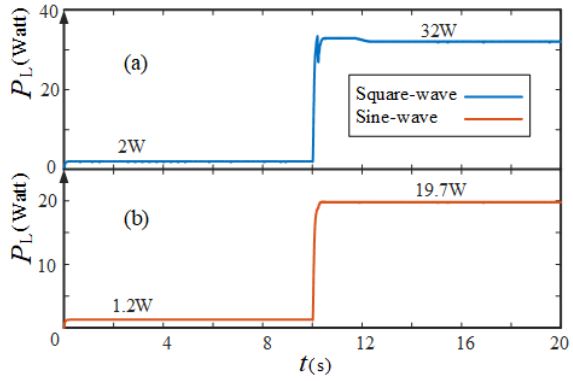

Fig. 21. Simulation results for output power P_L: (a) square-wave excitation (b) sine-wave excitation (The adaptive IM circuit is switched-on from t=10s).

The increase of power transferred as a result of square-wave excitation: The power transferred to the output load for square-wave and sine-wave excitations is depicted in Fig. 21(a) and (b), respectively. As seen, when applying a square-wave excitation, the amount of power transferred to the output load P_L is increased. The reason is that the amplitude of the first harmonic of a square-wave signal is $4/\pi$ times larger than the amplitude of the square-wave voltage. As an advantage, applying square-wave excitation results in $16/\pi^2$ ($\cong$ 1.62) times larger amount of transferred power to the output load (32-Watt for square-wave excitation compared to 19.7-Watt for sine-wave excitation.)

V. Comparison and Discussion

A. Frequency Splitting Analysis

Firstly, the frequency splitting analysis presented in literature are compared by that of this paper, in terms the following aspects, and the results are presented in Table IV.

1) Analysis Method Basis: To analyze frequency splitting phenomenon, most papers have employed either coupled mode theory (CMT), or circuit theory (CT). The CMT-based method is a physical approach that investigates the energy exchange process between two resonators [29]. However, it is only applicable to coupled-coils with high-quality (high-Q) factors or large coupling distances. Rather, the CT method utilized in this paper is based on the mutual inductance model with less complexity and computation [29]. Since it results in more accurate transient analysis, it is widely adopted.

2) Engineering Insight: Although expressions for frequency splitting were provided in several recent publications, this phenomenon still calls for more detailed physical analysis. In fact, only the mathematical descriptions on frequency splitting phenomenon were provided and from there, splitting characteristics and frequencies were extracted. There were no complete discussions on how/why the splitting phenomenon has appeared in the strongly-coupled region. Therefore, this paper provided an in-depth analysis of this phenomenon.

3) Resonant Topology: Based on series/parallel (S/P) compensation topologies in transmitter/receiver sides, there exist four WPT system types of SS, PP, PS, and SP. It has been mentioned that only SS and SP types show frequency splitting [30]. As the resonant frequency in the SS type is independent of the load and the coupling coefficient [29], this type is widely used in the WPT systems, and several pieces of research have been carried out to analyze and suppress the frequency splitting.

TABLE IV
Comparison Between Frequency Splitting Phenomenon Analysis Methods

Ref.	Analysis Method	Engineering insight	Coils	Resonant topology	Symmetrical/ Asymmetrical	Frequency
[13]	CT	NO	2	SS	Both	90.79kHz
[29]	CT and CMT	NO	2, 3, and 4	SS	Symmetrical	6.7MHz
[30]	CT	NO	2	SS	Symmetrical	85kHz
[31]	CMT	NO	2, 3, and 4	SS	Symmetrical	7MHz
[32]	CT	NO	2	SS	Symmetrical	12.3MHz
[33]	CT and CMT	NO	2	SS	Symmetrical	1MHz
[34]	CT	NO	2 and 4	SS	Symmetrical	10MHz
[35]	CT	NO	2	SS, SP, PS, and PP	Symmetrical	5MHz
[36]	CT	NO	4	SS	Symmetrical	3.87MHz
[37]	CT	NO	Mutiple-receiver	SS	Symmetrical	85kHz
[38]	CT	NO	2	SS	Both	6.78MHz
[39]	CT	NO	2, 3,...,N	SS	Symmetrical	13.3MHz
This paper	**CT**	**YES**	**2**	**SS**	**Symmetrical**	**125kHz**

B. IM Method

Here, the proposed IM method is compared with other methods in terms of efficiency, cost, converging speed, etc. The results are presented in Table V.

As discussed earlier, the maximum transferred-power happens at the resonant-frequency f_s which is a function of circuit resonant-elements (L_1, L_2, C_1, and C_2) and coupling-factor k or coil-to-coil distance. Thus, changing coil-to-coil distance causes an impedance mismatch at WPT systems' input, especially in the strongly-coupled region. To overcome this mismatch, there are two main methods presented in the literature.

The first method group is called frequency-tracking (FT), in which the frequency of input power supply is adaptively adjusted to the coil-to-coil distance by applying a feedback control [13], [16], and [30]. This causes the WPT system to operate at one of the splitting frequencies (f_{odd} or f_{even}), which may result in local maximum transferred power point (instead of global one) [13], [30]. Besides, Fig. 22 shows a significant decrease of efficiency η outside of the strongly-coupled region, which is another drawback of the FT-based method [18]. Further, FT-based methods may need additional circuits for wireless data transfer between the receiver and transmitter sides [16].

The second method group (known as IM method) changes the resonant frequency f_s of the coupled-coils to match with the power source frequency. This group includes coupling manipulation [11], [32], [40], [41], lossless LC circuits (IM networks) [1], [2], [9], [10], [23], [24], [42], [43], [44], and adaptive DC/DC converters [20], [45].

Coupling manipulation IM methods, such as non-identical resonant coil (NIRC) structure [40], anti-parallel resonant loops [11], and mixed electric and magnetic couplings [32] can inhibit the coupling coefficient from dramatic distance-related variations in the strongly-coupled region, without extra complex circuits. However, their robustness against coupling

TABLE V
COMPARISON BETWEEN DIFFERENT ADAPTIVE AUTOMATIC IM METHODS USING LOSSLESS LC CIRCUITS FOR MAXIMIZING WIRELESSLY TRANSMITTED POWER

Ref.	Description	Number of iterations	η	Complexity	Conversion speed	Cost	f_s
[1]	Automatic IM using L-matching circuit minimizing power reflection	Multiple	$\sim 85\%$	High	Medium	High	13.56 MHz
[2]	Real-time active IM using a variable circuit topology, including discrete passive and p-i-n diodes, designed by genetic algorithm (GA)	Multiple	–	Medium	Medium	Low	13.56 MHz
[9]	Switchable capacitor array circuit at transmitter side compensating for variation of coupling coefficient and minimizing power reflection	Multiple	$\sim 89\%$	High	Medium	Medium	370 kHz
[10]	Range-adaptive IM using alternative multiple loops reducing input impedance variation	Multiple	92%	High	Medium	Medium	13.56 MHz
[23]	Two-side adaptive IM strategy using multi-loop coils of various combinations minimizing power reflection	Multiple	81.8%	High	Medium	High	13.56 MHz
[24]	Automatically adjusting series resonant capacitors to keep the voltage-current phase difference zero	Multiple	49%	High	Low	High	13.56 MHz
[42]	Adaptive IM network reliant on a novel capacitor matrix dealing with frequency mismatch	Multiple	88%	High	Medium	Medium	13.56 MHz
[43]	Adaptive two-side IM network using self-tuned L-matching circuit maximizing η	Multiple	85.4%	High	Medium	High	17.1 MHz
[44]	Real-time range-adaptive multi-loop IM using a machine learning technique relient on neural networks reducing input impedance variation	Multiple	$\sim 90\%$	High	Medium	High	13.56 MHz
This paper	**An adaptive IM method obtaining optimal IM network parameters in single step by estimating input voltage amplitude V_{in}, active P_{in} and reactive power Q_{in}**	**Single**	$\sim 90\%$	**High**	**High**	**High**	**125 kHz**

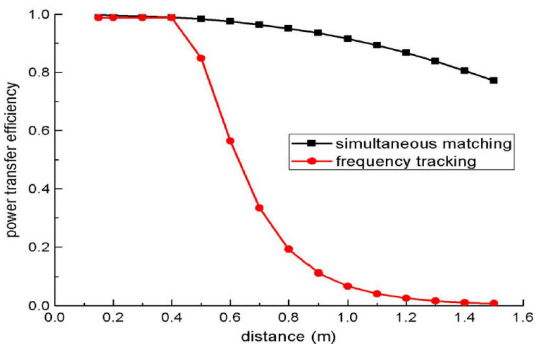

Fig. 22. Comparison of the power transfer efficiency using IM-based and frequency tracking-based methods [18].

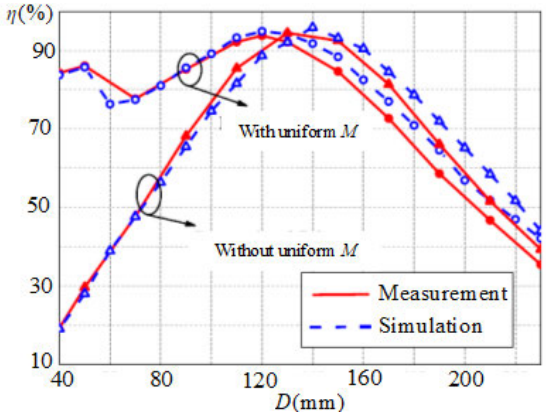

Fig. 23. Efficiency with and without uniform mutual inductance M profile [32].

variation may not be guaranteed in practice. Besides, as shown in Fig. 23, a uniform M profile may reduce the mutual inductance in the weakly-coupled region, which negatively affects the power transfer performance [32].

Although adaptive DC/DC converters eliminate the need for bulky IM circuits, they may impose additional power losses (i.e., switching and ohmic losses) [24].

Adaptive IM-based method, using IM networks holds the resonant-frequency constant. In this method, the WPT system is capable of adapting itself to any variation in coil-to-coil distance. This method, among all the mentioned methods, appears to be the most promising, because not only is it robust against coupling variation (due to its real-time impedance matching) but also is capable of delivering the global maximum transmitted power at any coil-to-coil distance.

Experimental results show that the proposed adaptive IM method improves the efficiency from less than 60% to around 90%, in the strongly-coupled region, at 125kHz. This method obtains the optimal IM network parameters in a single step, whereas the other IM based methods use search-and-find techniques. These techniques switch several inductors and capacitors by iterations before converging to the optimal values. Therefore, the proposed IM method outperforms others in terms of conversion speed. High conversion speed makes the proposed method a promising solution for the application with rapid variation in coupling distance, such as wireless charging of moving electric vehicles.

VI. CONCLUSION

This paper investigates the effect of coupling variations on a two-coil WPT system performance. In the strongly-coupled region, a large impedance-mismatch happens at the input of the WPT system. An adaptive real-time impedance matching method is proposed and verified by simulations and experiments to reduce this mismatch. The proposed method estimates the amplitude and phase of the input impedance.

This estimation is based on the magnitude of the WPT system input voltage and the average value of active power P_{in} and reactive power Q_{in}. Then, the parameters of the IM network are obtained by a straightforward calculation. The proposed method obtains optimal IM network parameters in one step, whereas traditional IM-based methods obtain these parameters through search-and-find techniques. The experimental results verify the effectiveness of the proposed method.

REFERENCES

[1] T. C. Beh, M. Kato, T. Imura, S. Oh, and Y. Hori, "Automated impedance matching system for robust wireless power transfer via magnetic resonance coupling," *IEEE Trans. Ind. Electron.*, vol. 60, no. 9, pp. 3689–3698, Sep. 2013.

[2] J. Bito, S. Jeong, and M. M. Tentzeris, "A real-time electrically controlled active matching circuit utilizing genetic algorithms for wireless power transfer to biomedical implants," *IEEE Trans. Microw. Theory Techn.*, vol. 64, no. 2, pp. 365–374, Feb. 2016.

[3] M. Taghadosi and H. Kassiri, "A real-time-link-adaptive operation scheme for maximum energy storage efficiency in resonant CM wireless power receivers," *IEEE Trans. Circuits Syst. I, Reg. Papers*, vol. 68, no. 1, pp. 510–523, Jan. 2021.

[4] A. Trigui et al., "Generic wireless power transfer and data communication system based on a novel modulation technique," *IEEE Trans. Circuits Syst. I, Reg. Papers*, vol. 67, no. 11, pp. 3978–3990, Nov. 2020.

[5] M. B. Lillholm, Y. Dou, X. Chen, and Z. Zhang, "Analysis and design of 10-MHz capacitive power transfer with multiple independent outputs for low-power portable devices," *IEEE J. Emerg. Sel. Topics Power Electron.*, vol. 10, no. 1, pp. 149–159, Feb. 2022.

[6] M. Vinod, D. Kishan, and B. D. Reddy, "Three-leg DC–DC converter for efficient inductive power transfer of electric vehicles for wide-range battery applications," *IEEE Trans. Power Electron.*, early access, Apr. 25, 2023, doi: 10.1109/TPEL.2023.3269886.

[7] A. Kuperman, "Simple enhancement of series–series-compensated inductive wireless power transfer links operating with load-independent voltage output at fixed frequency to attain zero inverter phase angle," *IEEE Trans. Power Electron.*, vol. 38, no. 5, pp. 5670–5674, May 2023.

[8] A. P. Sample, D. A. Meyer, and J. R. Smith, "Analysis, experimental results, and range adaptation of magnetically coupled resonators for wireless power transfer," *IEEE Trans. Ind. Electron.*, vol. 58, no. 2, pp. 544–554, Feb. 2011.

[9] J. Lee, Y. Lim, W. Yang, and S. Lim, "Wireless power transfer system adaptive to change in coil separation," *IEEE Trans. Antennas Propag.*, vol. 62, no. 2, pp. 889–897, Feb. 2014.

[10] J. Kim and J. Jeong, "Range-adaptive wireless power transfer using multiloop and tunable matching techniques," *IEEE Trans. Ind. Electron.*, vol. 62, no. 10, pp. 6233–6241, Oct. 2015.

[11] W. Lee, W. Son, K. Oh, and J. Yu, "Contactless energy transfer systems using antiparallel resonant loops," *IEEE Trans. Ind. Electron.*, vol. 60, no. 1, pp. 350–359, Jan. 2013.

[12] Y. Lyu et al., "A method of using nonidentical resonant coils for frequency splitting elimination in wireless power transfer," *IEEE Trans. Power Electron.*, vol. 30, no. 11, pp. 6097–6107, Nov. 2015.

[13] W. Niu, J. Chu, W. Gu, and A. Shen, "Exact analysis of frequency splitting phenomena of contactless power transfer systems," *IEEE Trans. Circuits Syst. I, Reg. Papers*, vol. 60, no. 6, pp. 1670–1677, Jun. 2013.

[14] F. Nasr, M. Madani, and M. Niroomand, "Precise analysis of frequency splitting phenomenon of magnetically coupled wireless power transfer system," in *Proc. IEEE Asia Pacific Microw. Conf. (APMC)*, Nov. 2017, pp. 219–224.

[15] B.-J. Jang, S. Lee, and H. Yoon, "HF-band wireless power transfer system: Concept, issues, and design," *Prog. Electromagn. Res.*, vol. 124, pp. 211–231, 2012.

[16] N. Y. Kim, K. Y. Kim, and C.-W. Kim, "Automated frequency tracking system for efficient mid-range magnetic resonance wireless power transfer," *Microw. Opt. Technol. Lett.*, vol. 54, no. 6, pp. 1423–1426, Jun. 2012.

[17] S. Huang, T. Lee, and T. Huang, "Inductive power transfer systems for PT-based ozone-driven circuit with flexible capacity operation and frequency-tracking mechanism," *IEEE Trans. Ind. Electron.*, vol. 61, no. 12, pp. 6691–6699, Dec. 2014.

[18] J. Park, Y. Tak, Y. Kim, Y. Kim, and S. Nam, "Investigation of adaptive matching methods for near-field wireless power transfer," *IEEE Trans. Antennas Propag.*, vol. 59, no. 5, pp. 1769–1773, May 2011.

[19] F. Nasr, S. M. Madani, and M. Niroomand, "Dual-objective control strategy for maximum power and efficiency point tracking in wirelessly powered biomedical implanted devices," *IET Microw., Antennas Propag.*, vol. 14, no. 1, pp. 36–44, Jan. 2020.

[20] Y. Huang, N. Shinohara, and T. Mitani, "Impedance matching in wireless power transfer," *IEEE Trans. Microw. Theory Techn.*, vol. 65, no. 2, pp. 582–590, Feb. 2017.

[21] N. Y. Kim, K. Y. Kim, J. Choi, and C.-W. Kim, "Adaptive frequency with power-level tracking system for efficient magnetic resonance wireless power transfer," *Electron. Lett.*, vol. 48, no. 8, pp. 452–454, Apr. 2012.

[22] H. Li, J. Li, K. Wang, W. Chen, and X. Yang, "A maximum efficiency point tracking control scheme for wireless power transfer systems using magnetic resonant coupling," *IEEE Trans. Power Electron.*, vol. 30, no. 7, pp. 3998–4008, Jul. 2015.

[23] B. Park and J. Lee, "Adaptive impedance matching of wireless power transmission using multi-loop feed with single operating frequency," *IEEE Trans. Antennas Propag.*, vol. 62, no. 5, pp. 2851–2856, May 2014.

[24] S. Iguchi, P. Yeon, H. Fuketa, K. Ishida, T. Sakurai, and M. Takamiya, "Wireless power transfer with zero-phase-difference capacitance control," *IEEE Trans. Circuits Syst. I, Reg. Papers*, vol. 62, no. 4, pp. 938–947, Apr. 2015.

[25] W. Zhong, S. Zhang, M. Chen, and M. D. Xu, "Reconfigurable resonant topology linking two-, three-, and four-coil modes for WPT with large coupling range and fixed frequency," *IEEE Trans. Power Electron.*, vol. 37, no. 7, pp. 8713–8725, Jul. 2022.

[26] A. Safaee and K. Woronowicz, "Time-domain analysis of voltage-driven series–series compensated inductive power transfer topology," *IEEE Trans. Power Electron.*, vol. 32, no. 7, pp. 4981–5003, Jul. 2017.

[27] M. Zhou, F. Liu, K. Lu, and X. Chen, "Modular stacked multiport wireless energy interconnection system with virtual AC bus and its power flow control strategy," *IEEE Trans. Power Electron.*, vol. 37, no. 12, pp. 15774–15784, Dec. 2022.

[28] F. Liu, X. Zhao, Z. Deng, and Y. Liu, "CryoSCA: A cryogenic switched capacitor waveform digitizer ASIC for the point-contact HPGe detectors," in *Proc. IEEE Nucl. Sci. Symp. Med. Imag. Conf. Proc. (NSS/MIC)*, Nov. 2018, pp. 1–4.

[29] X. Wei, Z. Wang, and H. Dai, "A critical review of wireless power transfer via strongly coupled magnetic resonances," *Energies*, vol. 7, no. 7, pp. 4316–4341, Jul. 2014.

[30] X. Liu, X. Yuan, C. Xia, and X. Wu, "Analysis and utilization of the frequency splitting phenomenon in wireless power transfer systems," *IEEE Trans. Power Electron.*, vol. 36, no. 4, pp. 3840–3851, Apr. 2021.

[31] W. Niu, W. Gu, J. Chu, and A. Shen, "Frequency splitting patterns in wireless power relay transfer," *IET Circuits, Devices Syst.*, vol. 8, no. 6, pp. 561–567, Nov. 2014.

[32] X. Y. Zhang, C. Xue, and J. Lin, "Distance-insensitive wireless power transfer using mixed electric and magnetic coupling for frequency splitting suppression," *IEEE Trans. Microw. Theory Techn.*, vol. 65, no. 11, pp. 4307–4316, Nov. 2017.

[33] L. Jianyu, T. Houjun, and G. Xin, "Frequency splitting analysis of wireless power transfer system based on T-type transformer model," *Electron. Electr. Eng.*, vol. 19, no. 10, pp. 109–113, Dec. 2013.

[34] R. Huang and B. Zhang, "Frequency, impedance characteristics and HF converters of two-coil and four-coil wireless power transfer," *IEEE J. Emerg. Sel. Topics Power Electron.*, vol. 3, no. 1, pp. 177–183, Mar. 2015.

[35] M. Iordache, A. Marinescu, I. G. Sîrbu, L. Mandache, D. Niculae, and L. Iordache, "New aspects on the frequency splitting and bifurcation phenomena in wireless power transfer systems," *Ann. Univ. Craiova, Elect. Eng. Ser.*, no. 40, pp. 46–53, 2016.

[36] Y. Zhang, Z. Zhao, and K. Chen, "Frequency-splitting analysis of four-coil resonant wireless power transfer," *IEEE Trans. Ind. Appl.*, vol. 50, no. 4, pp. 2436–2445, Jul. 2014.

[37] H. Nguyen and J. I. Agbinya, "Splitting frequency diversity in wireless power transmission," *IEEE Trans. Power Electron.*, vol. 30, no. 11, pp. 6088–6096, Nov. 2015.

[38] W. Choi, C. Park, and K. Lee, "Circuit analysis of achievable transmission efficiency in an overcoupled region for wireless power transfer systems," *IEEE Syst. J.*, vol. 12, no. 4, pp. 3873–3876, Dec. 2018.

[39] J. I. Agbinya and H. Nguyen, "Principles and applications of frequency splitting in inductive communications and wireless power transfer systems," *Wireless Pers. Commun.*, vol. 107, no. 2, pp. 987–1017, Jul. 2019.
[40] J. Lee, Y. Lim, H. Ahn, J. Yu, and S. Lim, "Impedance-matched wireless power transfer systems using an arbitrary number of coils with flexible coil positioning," *IEEE Antennas Wireless Propag. Lett.*, vol. 13, pp. 1207–1210, 2014.
[41] P. Hu, J. Ren, and W. Li, "Frequency-splitting-free synchronous tuning of close-coupling self-oscillating wireless power transfer," *Energies*, vol. 9, no. 7, p. 491, Jun. 2016.
[42] Y. Lim, H. Tang, S. Lim, and J. Park, "An adaptive impedance-matching network based on a novel capacitor matrix for wireless power transfer," *IEEE Trans. Power Electron.*, vol. 29, no. 8, pp. 4403–4413, Aug. 2014.
[43] S. D. Barman, A. W. Reza, N. Kumar, and T. I. Anowar, "Two-side impedance matching for maximum wireless power transmission," *IETE J. Res.*, vol. 62, no. 4, pp. 532–539, Jul. 2016.
[44] S. Jeong, T. Lin, and M. M. Tentzeris, "Range-adaptive impedance matching of wireless power transfer system using a machine learning strategy based on neural networks," in *IEEE MTT-S Int. Microw. Symp. Dig.*, Jun. 2019, pp. 1423–1425.
[45] D. Bui, T. M. Mostafa, A. P. Hu, and R. Hattori, "DC–DC converter based impedance matching for maximum power transfer of CPT system with high efficiency," in *Proc. IEEE PELS Workshop Emerg. Technol., Wireless Power Transf. (Wow)*, Jun. 2018, pp. 1–5.

Fatemeh Nasr Esfahani (Student Member, IEEE) received the B.Sc. and M.Sc. degrees in electrical engineering from the Amirkabir University of Technology, University of Isfahan, in 2015 and 2018, respectively. Her research interests include power electronics, electric vehicles, wireless power transfer, and renewable energies.

Seyed M. Madani (Senior Member, IEEE) received the B.Sc. degree from the Sharif University of Technology, Tehran, Iran, in 1989, the M.Sc. degree from the University of Tehran, Tehran, in 1991, and the Ph.D. degree from the Eindhoven University of Technology, Eindhoven, The Netherlands, in 1999, all in electrical power engineering. From 2000 to 2005, he was with Texas A&M University, College Station, TX, USA; the University of Puerto Rico, San Juan, Puerto Rico; and the University of Wisconsin, Madison, WI, USA, as an Assistant Professor or a Visiting Professor. From 2005 to 2011, he was with the Isfahan University of Technology, Isfahan, Iran, as an Assistant Professor. He is currently an Associate Professor of electrical power engineering with the University of Isfahan, Isfahan. His research interests include renewable energy, power electronics, power systems, and electrical machines.

Mehdi Niroomand (Member, IEEE) was born in Isfahan, Iran, in 1979. He received the B.S., M.S., and Ph.D. degrees in electrical engineering from the Isfahan University of Technology, Isfahan, in 2001, 2004, and 2010, respectively. Since 2010, he has been with the Department of Electrical Engineering, University of Isfahan, Isfahan, where he is currently an Associate Professor. His current research interests include power electronics, switching power supplies, control in power electronics, and renewable energies.

Alireza Safaee (Senior Member, IEEE) received the Ph.D. degree in power electronics from Queen's University in 2015. From 1997 to 2005, he was a Design Engineer/the Manager of Manabe Taghzyeh Electronic Company, where he played a major role in establishing automotive lighting products for national automakers. He has designed controllers for tail lights and brake lights, completed the standard compliance processes, and later launched the product lines. He also designed 10 kW inverters for emergency lightings of metro stations, with extreme safety and security considerations. These systems are still in operation. From 2011 to 2014, he was with Bombardier Transportation, working on projects that required lighting systems development (via collaboration with vendors) for rail wayside lighting and for train vehicle interior lighting. From 2014 to 2017, he was a Senior Key Expert with the Osram Sylvania Research Center, working on steerable automotive lighting systems, street lighting LED drivers that could energize the IoT sensing systems, micro LED displays, and tail lights for EVs. He has contributed to a first-of-a kind high-precision flicker measurement tool. His designs are used in several products and granted more than ten patents.